Journal of Geography and Geology; Vol. 7, No. 3; 2015
ISSN 1916-9779 E-ISSN 1916-9787
Published by Canadian Center of Science and Education

A Comparison of Land Surface Temperature, Derived from AMSR-2, Landsat and ASTER Satellite Data

Mukesh Singh Boori[1,2,3], Heiko Balzter[2], Komal Choudhary[3], Viktor Kovelskiy[3] & Vit Vozenilek[4]

[1] American Sentinel University, Colorado, USA

[2] Dept. of Geography, University of Leicester, England, UK

[3] Samara State Aerospace University, Samara, Russia

[4] Dept. of Geoinformatics, Palacky University Olomouc, Czech Republic

Correspondence: Mukesh Singh Boori, Samara State Aerospace University, 34, Moskovskoye Shosse, Samara 443086, Russia. Tel: 7-987-432-9875. E-mail: mukesh.boori@americansentinel.edu

Received: July 7, 2015 Accepted: August 26, 2015 Online Published: August 29, 2015

doi:10.5539/jgg.v7n3p61 URL: http://dx.doi.org/10.5539/jgg.v7n3p61

The research is financed by (European Union Social Fund, project: CZ.1.07/2.3.00/30.0041).

Abstract

Land surface parameters are highly integrated and have a direct effect on water and energy balance and weather predictions. Due to the difficulties in correcting the influences of the atmosphere absorbability and the earth surface emissivity diversification, the retrieval of land surface temperature (LST) from satellite data is a challenging task. To retrieve microwave land emissivity, infrared surface skin temperatures have been used as surface physical temperature. However, passive microwave emissions originate from deeper layers with respect to the skin temperature. So, this inconsistency in sensitivity depths between skin temperatures and microwave temperatures may introduce a discrepancy in the determined emissivity. In this research work, 6 sample sites were chosen on the globe for 2013 and 2014 and then derive land surface temperature from AMSR-2, Landsat and ASTER brightness temperature values. The algorithm is developed from a surface brightness temperature dataset, which uses a range of surface parameters and atmospheric quantities as inputs. The retrieved LST is compared within AMSR-2, Landsat and ASTER for the same period and area. Maximum time ASTER shows highest temperature than other data and AMSR-2 has lowest temperature on same area. Landsat and ASTER is closer to ground measured temperature than AMSR-2 data. It will be interesting to see how the satellite-derived surface temperature will behave in an assimilation scheme in a follow-up study.

Keywords: AMSR-2, ASTER, landsat data, brightness temperature

1. Introduction

Surface temperature is a key parameter in many energy balance applications such as evaporation modeling, climate models, and radiative transfer modelling (Maimaitiyiming et al., 2014; Norouzi et al., 2011). Land use/cover (in terms of temperature & soil moisture) effect surrounding climate such as water vapors, dust partials, gas molecules and clouds formation; so it's directly effect on rain and then land use/cover. By this way it`s effect whole ecosystem and correlate with natural disasters. Land Surface Models (LSMs) is expected to lead to improved short-term to long range weather forecasting capability. Because land surface parameters are highly integrated states, errors in land surface forcing, model physics and parameterization tend to accumulate in the land surface stores of these models, such as soil moisture and surface temperature (Boori et al., 2015a; McCollum & Ferraro, 2005). This has a direct effect on the models' water and energy balance calculations, and may eventually result in inaccurate weather predictions. Timely monitoring of natural disasters is important for minimizing economic losses caused by floods, drought, etc. so it's important for emergency management during natural disasters. That`s why remote sensing for land surface temperature has become an important research subject globally (Min et al., 2010).

Ground observations are generally useful for local applications; however, they are highly intensive in man-power and equipment costs. Furthermore, ground observations of land surface temperature are point measurements and

since variability can be high, especially in regions with discontinuous vegetation, scaling up to spatial averages is often difficult (Boukabara et al., 2007). In other side satellite-generated brightness temperatures (BT) are more convenient on global level and temporal basis (Entekhabi et al., 2010; Boori & Ferraro, 2015).

Instantaneous measures of microwave brightness temperature (BT) have been used in a variety of applications to estimate column water vapour abundance, rainfall rate, surface ocean wind speed, ocean salinity, soil moisture, freeze/thaw state, land surface temperature, inundation fraction, and vegetation structure (Zhang et al., 2010; Prigent et al., 2008; Norouzi et al., 2012; Boori et al., 2014; Njoku et al., 2003; Papa et al., 2006). Land surface properties can be inferred accurately if physical temperature and emissivity variations can be separated (Yang & Yang, 2006). Diurnal synoptic and variations of land surface temperature, as well as the atmospheric temperature and water vapour profiles, affect the observed BT. The more frequent the observation of BT throughout the day, the better understanding of the variability of retrieved parameters (Stephen et al., 2010).

There are very few studies that have dealt with the characterization of the BT diurnal variation over land. The diurnal variation of physical and brightness temperatures as a function of incident solar radiation has been modeled for the Tropical Rainfall Measuring Mission (TRMM) Microwave Imager (TMI) (Aires et al., 2004). The characteristics of the skin temperature diurnal cycles as measured from IR over different land types were investigated. In densely vegetated areas with more moisture, skin temperature exhibits a smaller diurnal variation than in arid and desert areas (Chen et al., 2011).

The paper is organized in the sections below. Following the description of the study area in Section 2, brief discussion about datasets in section3, the methodology of calculating LST, and a brief introduction to normalized mutual information measure are presented in Section 4. The analysis and conclusions are presented in Sections 5 – 6, respectively.

2. Study Area

The study area has six training sites on globe in different continent to compare temperature in different satellites datasets on same location (Figure 1). Sample sites are located on following place: (1) Karl Stefan Memorial Airport (USA); (2) Mondai, Santa Catarina (Brazil); (3) Belgrade, Serbia (Europe); (4) Khartoum, Sudan (Africa); (5) Chengdu, China; (6) Kalgoorlie, Australia.

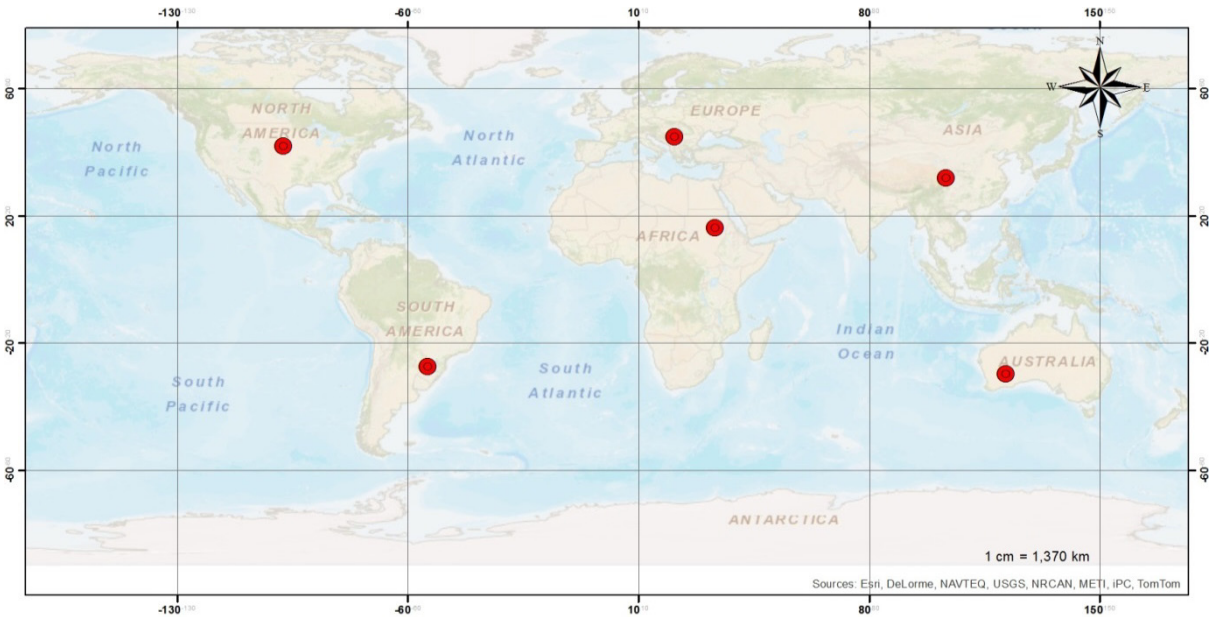

Figure 1. Observed data taken stations located on globe

3. Data Seta

This research work used thermal band of AMSR-2, Landsat and ASTER satellite data. Few specific characteristics of used satellite data are following:

AMSR2: The Advanced Microwave Scanning Radiometer - 2 (AMSR-2) on board the GCOM-W1 satellite is a remote sensing instrument for measuring weak microwave emission from the surface and the atmosphere of the

Earth. From about 700 km above the Earth, AMSR-2 provides highly accurate measurements of the intensity of microwave emission and scattering. The antenna of AMSR-2 rotates once per 1.5 seconds and obtains data over a 1450 km swath. This conical scan mechanism enables AMSR-2 to acquire a set of daytime and night time data with more than 99% coverage of the earth every 2 days. It's had 7 frequencies with vertical and horizontal polarizations. Here 36.5 GHz vertical frequency was used for land surface temperature, get from Japan Aerospace Exploration Agency. The 36.5 GHz AMSR-2 footprint is an oval of 25 km square, where the derived surface temperature fields are resampled in a 0.25 degree grid. A subset covering the sample sites is cut from the global dataset. The choice for these location is motivated by the presence of sets of observational data for the corresponding period of time (i.e. year 2013-14) and there availability. Observed data is collected from 6 stations located on globe (Figure 1), spatially representative of different types of land cover (Boori et al., 2015b).

Landsat: In this research work Landsat 8 satellite data was used. Landsat 8 carries two instruments: The Operational Land Imager (OLI) sensor and Thermal Infrared Sensor (TIRS) sensor. The TIRS sensor provides two thermal bands. These sensors provide improved signal-to-noise (SNR) radiometric performance quantized over a 12-bit dynamic range. This translates into 4096 potential grey levels in an image compared with only 256 grey levels in previous 8-bit instruments. Improved signal to noise performance enable better characterization of land cover state and condition (Fily et al., 2003). This product is delivered as 16-bit images (scaled to 55,000 grey levels). For this research work band number 11TIRS (11.5-12.51 μm) 100 m was used for surface temperature.

ASTER: ASTER data provides the user community with standard data products throughout the life of the mission. Algorithms to compute these products were created by the ASTER science team, and are implemented at the Land Processes Distributed Active Archive Centre (LP DAAC). Users can search and browse these products through GDS and NASA Reverb. For this research work band number 14 TIR (10.95 - 11.65 μm) was used for surface temperature. Its have 16 bit data with +/-8.55 telescope pointing capacity (Karbou et al., 2006).

4. Method

In our previous study (Boori et al., 2015c), we estimated microwave land surface emissivity over the globe from AMSR-E observations at all frequencies and both polarizations. The previous emissivity retrieval is based on the assumption that the infrared skin temperature is the effective physical temperature, which is equivalent to assuming that the microwave brightness temperature originates from the skin. This assumption is not necessarily true, but necessary because of a lack of general global information on penetration depth and temperature profile.

A physical model was proposed (Tedesco & Kim, 2006) to account for the effect of penetration depth on emissivity retrievals by revising the physical temperature. In this research work, first take sample sites and then derive land surface temperature from satellite brightness temperature by the help of following scaling factors for different satellite data (Wilheit et al., 2003):

AMSR-2: For AMSR2 data scale factor is set as 0.01[K]. For instance, if brightness temperature data is stored as 28312, original value of the data is 283.12[K].

ASTER: ASTER surface temperatures are computed from spectral radiance so begins by converting DNs to radiance and for that equation is following:

$$L_\lambda = (DN - 1) \text{ X } UCC$$

Where L_λ is the spectral radiance, DN are the TIR band digital numbers, and UCC are the published Unit Conversion Coefficients (0.005225 $w/m^{-2}/sr^{-1}/\mu m^{-1}$).

Temperature (measured in degrees Kelvin) is then given by:

$$T = K2 / (\ln (K1/ L_\lambda + 1)$$

Where K1 (641.32) and K2 (1271.22) are constants derived from Planck's radiance function.

Landsat: OLI and TIRS band data can be converted to TOA spectral radiance using the radiance rescaling factors provided in the metadata file:

$$\mathbf{L_\lambda = M_L Q_{cal} + A_L}$$

where:

$\mathbf{L_\lambda}$ = TOA spectral radiance ($w/m^{-2}/sr^{-1}/\mu m^{-1}$)
$\mathbf{M_L}$ = Band-specific multiplicative rescaling factor from the metadata (RADIANCE_MULT_BAND_x, where x is the band number)
$\mathbf{A_L}$ = Band-specific additive rescaling factor from the metadata (RADIANCE_ADD_BAND_x, where x is the

band number)
Q_{cal} = Quantized and calibrated standard product pixel values (DN)

TIRS band data can be converted from spectral radiance to brightness temperature using the thermal constants provided in the metadata file:

$$T = K2 / (\ln (K1/ L_\lambda + 1)$$

where:

T = At-satellite brightness temperature (K)
L_λ = TOA spectral radiance ($w/m^{-2}/sr^{-1}/\mu m^{-1}$)
K_1 = Band-specific thermal conversion constant from the metadata (K1_CONSTANT_BAND_x, where x is the band number, 10 or 11)
K_2 = Band-specific thermal conversion constant from the metadata (K2_CONSTANT_BAND_x, where x is the band number, 10 or 11)

5. Results

In the following section, 1°×1° spatial subsets of the products were co-registered so that the resulting subsets cover the same area as the Landsat, ASTER and AMSR-2 images in Figure 2-4. Where necessary, spatial re-sampling was performed using the 'nearest neighbour' method. The gravel plains are highly homogenous in space and time and outside globe two seasons (around September and June) the chances for precipitation are remote therefore, it is safe to assume that the land surface was completely dry for the results presented in this paper. The following section briefly discusses the actual land surface temperature on the same area and time from different satellite data sates (Figure 2-4).

AMSR-2: Figure 2 shows an example of the AMSR-2 surface temperature retrievals at day time in June 2014 and September 2013, which observational data are sampled.

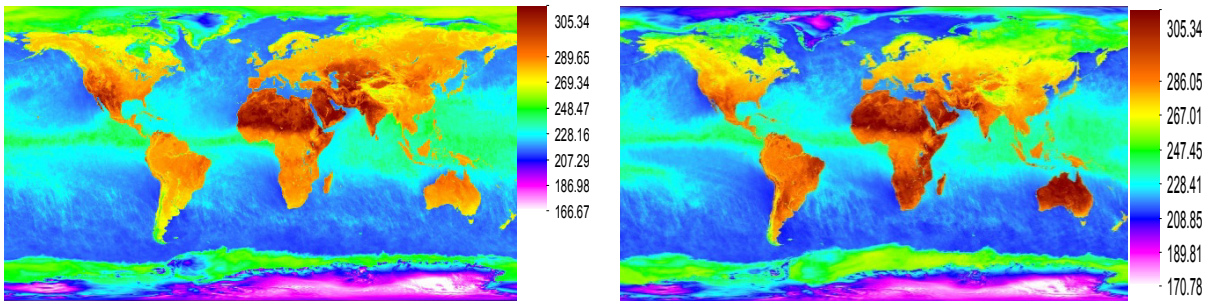

AMSR-2 06_2014 AMSR-2 09_2013

Figure 2. AMSR-2 data land surface temperature on globe

AMSR-2 June 2014 data show minimum 166.67 K and highest 305.34 K temperature and for September 2013 minimum is 170.78 K and highest is 305.34 K temperature. In June highest temperature is present in Sahara desert, west centre of North America and northeast part of Brazil, west part of India and china. In September 2013 is the same like 2014 but high temperature is also present in Australian desert, reduce area in India and China but increase in South Africa and South America (Figure 2).

Landsat: In 2014 sample site in Europe, Landsat 8 band number 11 shows 267.11 K as lowest temperature and 312.92 highest temperatures. Maximum region show around 290 to 300 k temperatures. In North America its 287.73 to 310.57 K and in South America is 274.34 to 293.71 K but maximum region have high temperature, above than 285 k (Figure 3).

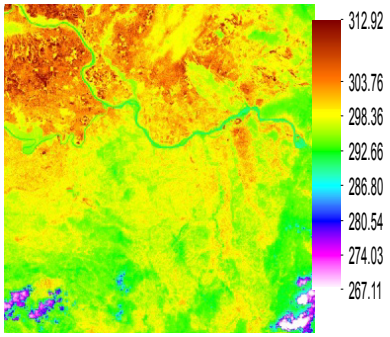

Landsat Surface Europe Temperature Kelvin 06_2014

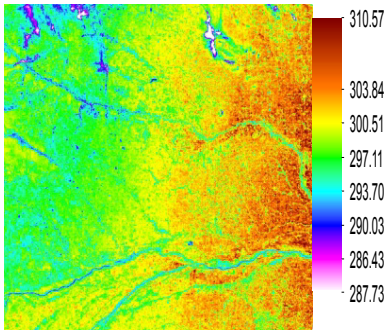

Landsat Surface North America Temperature Kelvin 06_2014

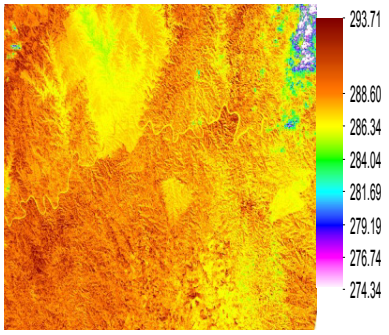

Landsat Surface South America Temperature Kelvin 06_2014

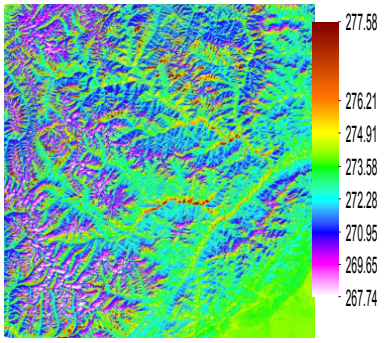

Landsat Surface Asia Temperature Kelvin 09_2013

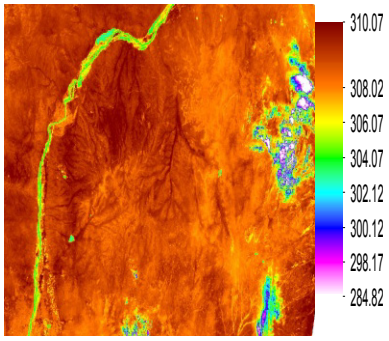

Landsat Surface Africa Temperature Kelvin 09_2013

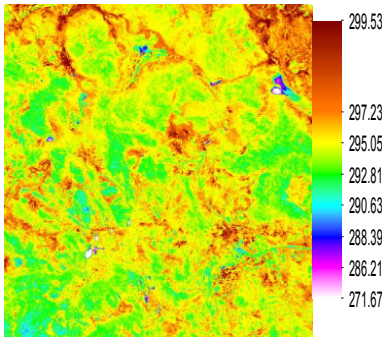

Landsat Surface Australia Temperature Kelvin 09_2013

Figure 3. Landsat data land surface temperature on sample site on globe

In 2013 in Australia temperature range is in between 271.67 to 299.53 K and this region show an average temperature. For Africa its 284 to 310 but maximum area have above than 305 K temperature, which show high temperature. In Asia it's from 267.74 to 277.58 K and maximum area has average temperature (Figure 3).

ASTER: In ASTER data on same location in 2014 in Europe, temperature range is in between 289.31 to 318.16 K and for North America is from 277.88 to 300.22 K. In both regions, maximum area is cool. In South America and Asia temperature range is 277.88 to 300.22 K and 256.85 to 300.68 K respectively. Maximum area has average temperature. In Africa and Australia it`s 275.14 to 320.80 and 285.79 to 303.80 K respectively (Figure 4).

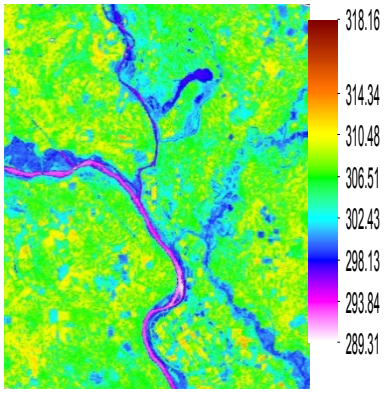

ASTER Europe 06_2014

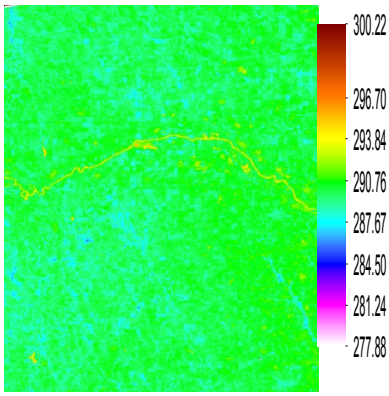

ASTER North America 06_2014

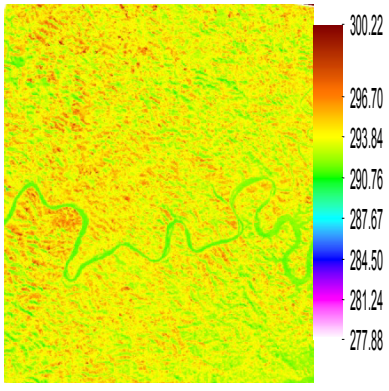

ASTER South America 06_2014

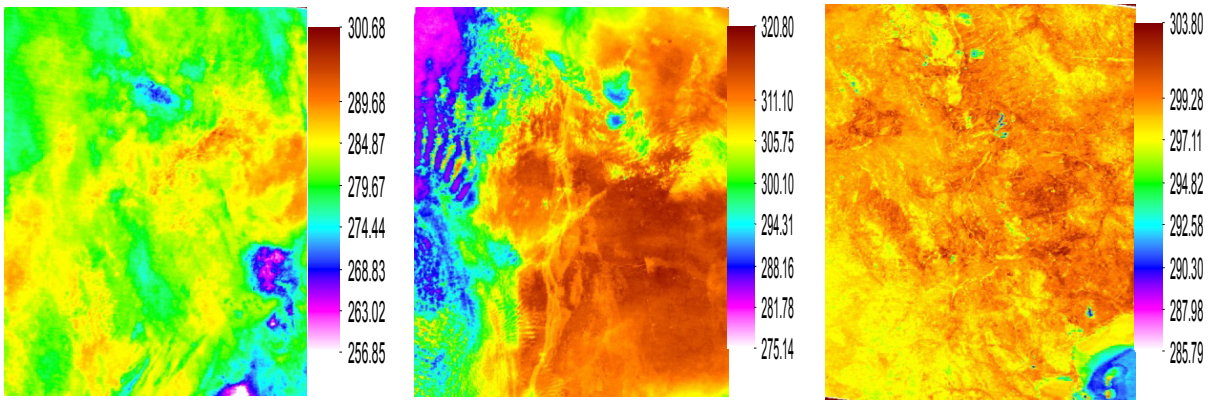

ASTER Asia 09_2013 ASTER Africa 09_2013 ASTER Australia 09_2013

Figure 4. ASTER data land surface temperature on sample site on globe

6. Comparing in Land Surface Temperature in AMSR-2, Landsat and ASTER Satellite Data:

In North America Landsat data showing highest and AMSR-2 data is showing lowest temperature in all locations. ASTER data temperature values are in between in North America. In South America ASTER show highest temperature and AMSR-2 lowest and Landsat is in between (Figure 5). For Europe is same like South America (table 1). In Africa Landsat have highest and AMSR-2 lowest temperature and ASTER data temperature is in between. In Asia ASTER is highest, than Landsat and AMSR-2 is the lowest temperature. For Australia, Highest is AMSR-2 than ASTER and Landsat is lowest temperature (Figure 5). The analysis results show that Landsat and ASTER data temperature is close to ground measurements in compare of AMSR-2 data temperature due to their high resolution and scale (table 1 & 2).

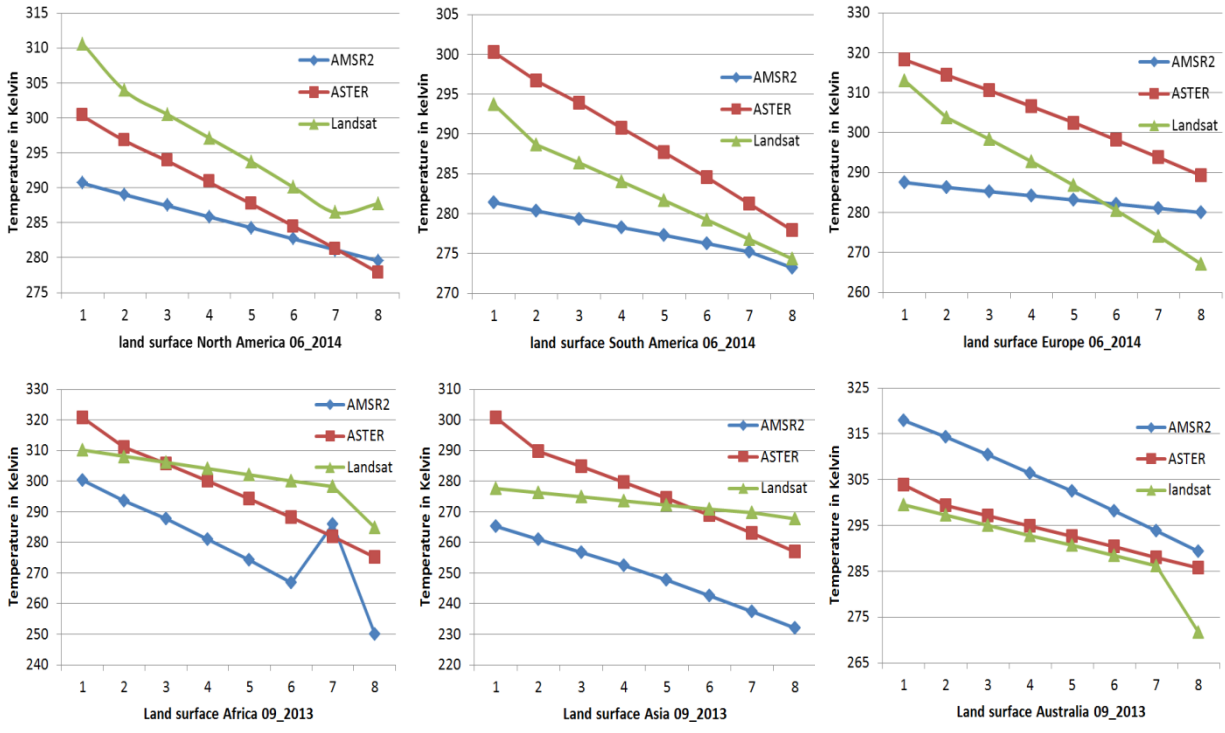

Figure 5. Comparing land surface temperature in ASTER, Landsat and AMSR-2 data

Table 1. Sensor measured temperature in kelvin

AMSR2 Te	ASTER Tem. K	Landsat Tem. K
North America 06_2014		
290.63	300.22	310.57
288.99	296.7	303.84
287.43	293.84	300.51
285.83	290.76	297.11
284.27	287.67	293.7
282.67	284.5	290.03
281.11	281.24	286.43
279.55	277.88	287.73
South America 06_2014		
281.39	300.22	293.71
280.33	296.7	288.6
279.32	293.84	286.34
278.28	290.76	284.04
277.27	287.67	281.69
276.23	284.5	279.19
275.23	281.24	276.74
273.16	277.88	274.34
Europe 06_2014		
287.44	318.16	312.92
286.33	314.34	303.76
285.27	310.48	298.36
284.19	306.51	292.66
283.14	302.43	286.8
282.06	298.13	280.54
281.01	293.84	274.03
279.95	289.31	267.11

AMSR2 Te	ASTER Tem. K	Landsat Tem. K
Africa 09_2013		
300.22	320.8	310.07
293.6	311.1	308.02
287.6	305.75	306.07
281.07	300.1	304.07
274.3	294.31	302.12
266.75	288.16	300.12
285.87	281.78	298.17
250.07	275.14	284.82
Asia 09_2013		
265.13	300.68	277.58
260.93	289.68	276.21
256.75	284.87	274.91
252.36	279.67	273.58
247.71	274.44	272.28
242.63	268.83	270.95
237.47	263.02	269.65
232.05	256.85	267.74
Australia 09_2013		
317.96	303.8	299.53
314.34	299.28	297.23
310.48	297.11	295.05
306.44	294.82	292.81
302.43	292.58	290.63
298.13	290.3	288.39
293.76	287.98	286.21
289.31	285.79	271.67

Table 2. Ground measured temperature in kelvin

North America:	302.10 – 289.10	South America:	293.1 – 288.10	Europe:	303.10 - 289.10
Asia:	300.10 – 268.10	Africa	311.10 – 296.10	Australia:	302.10 – 285.10

7. Conclusions

Evaluation of different data sources of surface temperature indicates that satellite derived passive microwave surface temperature is not necessarily a superior estimate compared to simulated surface temperature, if evaluated against a data set of observed point measurements. In general, data assimilation systems take into account observational errors and are able, despite errors in the observations, to obtain improvement of land surface temperature results, as long as the temporal trends are well represented. This research work show that Landsat and ASTER is close to ground measurements in compare of AMSR-2 data due to their high resolution and scale (Boori & Vozenilek, 2014).

It should be pointed out that the atmospheric forcing data sets used in the present study are mainly reanalysis data making use of in-situ observations. As a consequence, the simulations over the globe with a dense observation network are relatively accurate. However, no or little observation data are available for all sample sites and the quality of the forcing data and the simulations decreases. Hence, in these areas more scope is present for remote sensing data to constrain this type of research (Lambin & Ehrlich, 1997).

A further consideration is that the retrieval of passive microwave satellite derived surface temperature is hampered by weather conditions: frozen soil conditions in winter and (precipitating) clouds in summer. These phenomena appear to put some emphasis on ‘near’ in the assessment of the passive microwave retrieval of surface temperature as a ‘near all- weather’ technique. Consequently, this also applies to the passive microwave

soil moisture algorithm retrieval, in case the passive microwave surface temperature estimate is used Prigent et al., 1999).

Acknowledgments

The authors grate fully acknowledges the support by the Operational Program Education for Competitiveness - European Social Fund (project CZ.1.07/2.3.00/30.0041 of the Ministry of Education, Youth and Sports of the Czech Republic). The author is also thankful to Russian Scientific Foundation (RSF), grant no. 14-31-00014 "Establishment of a Laboratory of Advanced Technology for Earth Remote Sensing".

References

Aires, F., Prigent, C., & Rossow, W. B. (2004). Temporal interpolation of global surface skin temperature diurnal cycle over land under clear and cloudy conditions. *Journal of Geophysical Research-Atmospheres, 109*.

Boori, M. S., & Amaro, V. E. (2010). Land use change detection for environmental management:using multi-temporal, satellite data in Apodi Valley of northeastern Brazil. *Applied GIS, 6*(2), 1-15.

Boori, M. S., & Vozenilek, V. (2014). Land-cover disturbances due to tourism in Jeseniky mountain region: A remote sensing and GIS based approach. *SPIE Remote Sensing*, 9245, 92450T: 01-11. http://dx.doi.org/10.1117/12.2065112

Boori, M. S., & Ferraro, R. R. (2015). Global Land Cover classification based on microwave polarization and gradient ratio (MPGR). Geo-informatics for Intelligent Transportation. *Springer International Publishing Switzerland, 71*, 17-37. http://dx.doi.org/10.1007/978-3-319-11463-7-2

Boori, M. S., Netzband, M., Vozenilek, V., & Choudhary, K. (2015). Urban growth in last three decades in Kuala Lumpur, Malaysia IEEE: Urban Remote Sensing Event (JURSE), 2015 Joint, 01–04. http://dx.doi.org/10.1109/JURSE.2015.7120536

Boori, M. S., Vozenilek, V., & Burian, J. (2014). Land-cover disturbances due to tourism in Czech Republic. Advances in Intelligent Systems and Computing. *Springer International Publishing Switzerland*. ISSN 2194-5357. 303, 63-72. http://dx.doi.org/10.1007/978-3-319-08156-4-7

Boori, M. S., Vozenilek, V., & Choudhary, K. (2015). Exposer intensity, vulnerability index and landscape change assessment in Olomouc, Czech Republic, ISPRS: Int. Arch. Photogramm. Remote Sens. *Spatial Inf. Sci., XL*(7/W3), 771-776. http://dx.doi.org/10.5194/isprsannals-II-8-77-2014

Boori, M. S., Vozenilek, V., & Choudhary, K. (2015). Land use/cover disturbances due to tourism in Jeseniky Mountain, Czech Republic: A remote sensing and GIS based approach. *The Egyptian Journal of Remote Sensing and Space Sciences*, *18*(1), 17–26. http://dx.doi.org/10.1016/j.ejrs.2014.12.002

Boukabara, S. A., Weng, F. Z., & Liu, Q. H. (2007). Passive microwave remote sensing of extreme weather events using NOAA-18 AMSUA and MHS. *IEEE Transactions on Geoscience and Remote Sensing, 45*, 2228–2246.

Chen, S., Chen, X., Chen, W., Su, Y., & Li, D. (2011). A simple retrieval method of land surface temperature from AMSR-E passive microwave data – A case study over Southern china during the strong snow disaster of 2008. *International Journal of Applied Earth Observation and Geoinformation, 13*, 140-151.

Entekhabi, D., Njoku, E. G., O'Neill, P. E., Kellogg, K. H., Crow, W. T., & Edelstein, W. N. (2010). The soil moisture active passive (SMAP) mission. *Proceedings of the IEEE, 98*, 704–716.

Fily, M., Royer, A., Goita, K., & Prigent, C. (2003). A simple retrieval method for land surface temperature and fraction of water surface determination from satellite microwave brightness temperatures in sub-arctic areas. *Remote Sensing of Environment, 85*, 328–338.

Karbou, F., Gerard, E., & Rabier, F. (2006). Microwave land emissivity and skin temperature for AMSU-A and -B assimilation over land. *Quarterly Journal of the Royal Meteorological Society, 132*, 2333–2355.

Lambin, E. F., & Ehrlich, D. (1997). Land cover change in sub-saharan Africa (1982-1991): Application of a change index based on remote sensing surface temperature and vegetation indices at a continental scale. *Remote Sensing Environs, 61*, 181-200.

Maimaitiyiming, M., Ghulm, A., Tiyip, T., Pla, F., Carmona, P. L., Halik, U, Sawut, M., & Caetano, M. (2014). Effect of green space apatial pattern on the land surface temperature: Implications for sustainable urban planning and climate change adaptation. *ISPRS Journal of Photogramatry and Remote Sensing, 89*, 59-66.

McCollum, J. R., & Ferraro, R. R. (2005). Microwave rainfall estimation over coasts. *Journal of Atmospheric*

and Oceanic Technology, 22, 497–512.

Min, Q. L., Lin, B., & Li, R. (2010). Remote sensing vegetation hydrological states using passive microwave measurements. *IEEE Journal of Selected Topics in Applied Earth Observations and Remote Sensing, 3*, 124–131.

Njoku, E. G., Jackson, T. J., Lakshmi, V., Chan, T. K., & Nghiem, S. V. (2003). Soil moisture retrieval from AMSR-E. *IEEE Transactions on Geoscience and Remote Sensing, 41*, 215–229.

Norouzi, H., Rossow, W., Temimi, M., Prigent, C., Azarderakhsh, M., Boukabara, S., & Khanbilvardi, R. (2012). Using microwave brightness temperature diurnal cycle to improve imissivity retrievals over land. *Remote Sensing of Environment, 123*, 470-442.

Norouzi, H., Temimi, M., Rossow, W. B., Pearl, C., Azarderakhsh, M., & Khanbilvardi, R. (2011). The sensitivity of land emissivity estimates from AMSR-E at C and X bands to surface properties. *Hydrology and Earth System Sciences, 15*, 3577–3589.

Papa, F., Prigent, C., Rossow, W. B., Legresy, B., & Remy, F. (2006). Inundated wetland dynamics over boreal regions from remote sensing: the use of Topex-Poseidon dual-frequency radar altimeter observations. *International Journal of Remote Sensing, 27*, 4847–4866.

Prigent, C., Jaumouille, E., Chevallier, F., & Aires, F. (2008). A parameterization of the microwave land surface emissivity between 19 and 100 GHz, anchored to satellitederived estimates. *IEEE Transactions on Geoscience and Remote Sensing, 46*, 344–352.

Prigent, C., Rossow, W. B., Matthews, E., & Marticorena, B. (1999). Microwave radiometric signatures of different surface types in deserts. *Journal of Geophysical Research-Atmospheres, 104*, 12147–12158.

Stephen, H., Ahmad, S., & Piechota, T. C. (2010). Land surface brightness temperature modeling using solar insolation. *IEEE Transactions on Geoscience and Remote Sensing, 48*, 491–498.

Tedesco, M., & Kim, E. J. (2006). Retrieval of dry-snow parameters from microwave radiometric data using a dense-medium model and genetic algorithms. *IEEE Transactions on Geoscience and Remote Sensing, 44*, 2143–2151.

Wilheit, T., Kummerow, C. D., & Ferraro, R. (2003). Rainfall algorithms for AMSR-E. *IEEE Transactions on Geoscience and Remote Sensing, 41*, 204–214.

Yang, H., & Yang, Z. (2006). A modified land surface temperature split window retrieval algorithm and its applications over China. *Global and Planetary Change, 52*, 207-215.

Zhang, L. X., Zhao, T. J., Jiang, L. M., & Zhao, S. J. (2010). Estimate of phase transition water content in freeze-thaw process using microwave radiometer. *IEEE Transactions on Geoscience and Remote Sensing, 48*, 4248–4255.